Can. Aeronaut. Space J., Vol. 58, No. 1, pp. 47–59, 2012

Trajectory tracking control of flexible-joint space manipulators

S. Ulrich and J.Z. Sasiadek

Abstract. Operational problems with robots in space relate to several factors. One of the most important factors is the elastic vibrations in the joints. In this paper, control strategies for endpoint tracking of a 12.6 m × 12.6 m trajectory by a two-link space robotic manipulator are reviewed. Initially, a manipulator with rigid joints is actuated using a transpose jacobian control law and a model reference adaptive control system that adapts, in real-time, the control gains in response to errors between the actual system outputs and the ideal system outputs defined by a reference model. The rigid-joint dynamics model was pursued further to study a manipulator with flexible joints modeled with linear- and nonlinear-joint stiffness models. Then, the two rigid-joint control schemes were modified using the singular perturbation-based theory and applied for the control of both linear and nonlinear flexible-joint robot models. Finally, the rigid and flexible control systems described in this paper were evaluated in numerical simulations. Simulation results suggested that greatly improved tracking accuracy can be achieved by applying the adaptive control strategies.

Résumé. Les problèmes opérationnels avec les robots dans l'espace sont reliés à plusieurs facteurs, l'un des plus importants étant les vibrations élastiques dans les joints. Dans cet article, on examine les stratégies de commande pour le suivi du point d'équilibre d'une trajectoire de 12,6 m × 12,6 m par un robot manipulateur spatial à deux liens. Au départ, un manipulateur avec des joints rigides est actionné en ayant recours à une loi de commande jacobienne transposée et un système modèle de commande adaptatif de référence qui adapte en temps réel les gains de commande en réponse aux erreurs entre les sorties du système et les sorties du système idéales définies par un modèle de référence. Le modèle dynamique des joints rigides est examiné plus en profondeur pour étudier un manipulateur avec des joints flexibles modélisés à l'aide de modèles linéaires et non-linéaires de rigidité des joints. Ensuite, les deux procédures de commande à joints rigides sont modifiées en utilisant la théorie des perturbations singulières puis appliquées à la commande des modèles linéaires et non-linéaires de robot à joints flexibles. Enfin, les systèmes de commande rigides et flexibles décrits dans cet article sont évalués en simulations numériques. Les résultats de simulation suggèrent qu'il est possible d'obtenir des résultats nettement supérieurs en appliquant les stratégies de commande adaptatives.
[Traduit par la Rédaction]

Nomenclature

a_{sw}	soft-windup coefficient
$\mathbf{a}_1, \mathbf{a}_2$	stiffness coefficient matrices
$\mathbf{C}(\mathbf{q}, \dot{\mathbf{q}})$	Coriolis–centrifugal matrix
e_x, e_y	reference model endpoint position tracking error
$\boldsymbol{f}(\dot{\mathbf{q}})$	friction torque vector
$\mathbf{J}_m$	motor inertia matrix
$\mathbf{J}(\mathbf{q})$	Jacobian matrix
$\mathbf{k}$	joint stiffness matrix
$\mathbf{k}(\mathbf{q}, \mathbf{q_m})$	nonlinear-joint stiffness matrix
$\mathbf{K}_d$	derivative gain matrix
$\mathbf{K}_d(t)$	adaptive derivative gain matrix
$\mathbf{K}_{di}(t)$	integral component of adaptive derivative gain matrix
$\mathbf{K}_{dp}(t)$	proportional component of adaptive derivative gain matrix
$\mathbf{K}_p$	proportional gain matrix
$\mathbf{K}_p(t)$	adaptive proportional gain matrix
$\mathbf{K}_{pi}(t)$	integral component of adaptive proportional gain matrix
$\mathbf{K}_{pp}(t)$	proportional component of adaptive proportional gain matrix
$\mathbf{k}_{sw}$	soft-windup coefficient matrix
$\mathbf{K}_{sw}(\mathbf{q}, \mathbf{q}_m)$	soft-windup correction factor
$\mathbf{K}_v$	control gain matrix
L	Lagrange function
l_i	length of link, $i = 1, \ldots, n$
$\mathbf{M}(\mathbf{q})$	inertia matrix
m_i	nmass of link, $i = 1, \ldots, n$
$\mathbf{q}$	generalized coordinates vector
q_i	generalized coordinates, $i = 1, \ldots, n$
$\mathbf{S}$	inertial coupling matrix
T_r	kinetic energy of rigid robot

Received 16 September 2011. Revised 12 January 2012. Published on the Web at http://pubs.casi.ca/journal/casj on 4 April 2012.

S. Ulrich.[1] Ph.D. Candidate, Department of Mechanical and Aerospace Engineering, Carleton University, 1125 Colonel By Drive, Ottawa, ON K1S 5B6, Canada.

J. Z. Sasiadek. Professor, Department of Mechanical and Aerospace Engineering, Carleton University, 1125 Colonel By Drive, Ottawa, ON K1S 5B6, Canada.

[1]Corresponding author (e-mail: sulrich@connect.carleton.ca).

U_e	elastic potential energy of flexible joints
U_r	potential energy of rigid robot
x, y	actual endpoint position
x_c, y_c	commanded endpoint position
x_e, y_e	endpoint position tracking error
x_{ref}, y_{ref}	reference model endpoint position
γi	friction component parameters, $i = 1, \ldots, n$
Γ_{pp}, Γ_{pi}, Γ_{dp}, Γ_{di}	control parameters
ω_n	reference model natural frequency
σ_p, σ_d	control coefficients
τ	control torque vector
τ_f	fast control torque vector
τ_s	slow control torque vector
ζ	reference model damping ratio

Introduction

As early as the 1980s, the National Aeronautics and Space Administration (NASA) realized the importance of on-orbit servicing (OOS) for protecting their assets in space. On-orbit servicing refers to the maintenance of space systems in orbit, such as the maintenance, repair, assembly, refuelling, or upgrade of spacecraft after their deployment (Ellery, 2000). Besides servicing the Hubble Space Telescope most of the robotic servicing technologies have been driven by the International Space Station (ISS) program requirements. Over the years, a number of cargo-handling manipulators designed to operate on the ISS have been developed by international space agencies. Jointly developed by Canada and NASA, the main ISS robotic system, known as the ISS Mobile Servicing System, comprises the Space Station Remote Manipulator (SSRMS), the Special Purpose Dexterous Manipulator (SPDM), and the Mobile Remote Servicer Base System that acts as a movable platform for the SSRMS and SPDM (Salaberger, 1998). The Japanese Experiment Module Remote Manipulator System, built by the Japan Aerospace Exploration Agency, is a robotic manipulator system intended for supporting experiments to be conducted on the Japanese Experiment Module Exposed Facility at the ISS. Another space robotic manipulator is the European Robotic Arm which was developed by the European Space Agency. This robotic system consists of an 11 m manipulator with seven degrees of freedom (DOFs) and two booms scheduled to be attached to the Russian segment of the ISS in 2012. Originally designed for deployment and retrieval of large payloads, these cargo-handling robotic systems have proven their versatility, from serving as a platform for extra vehicular activities to performing inspection operations.

Worldwide space robotic activities currently concentrate on the development of lightweight and autonomous robotic manipulators designed specifically for advanced and complex OOS operations (Reintsema et al., 2007). In particular, the German Aerospace Center (DLR) Lightweight Robot III and the Robotics Component Verification on the International Space Station (ROKVISS) experiment were designed to test new lightweight robot components (**Figure 1**), such as harmonic drives, which are likely to be used on future unmanned space missions (DLR, 2010).

Originally developed for military applications, harmonic drives are mechanisms that are increasingly becoming popular for use in space applications owing to their low backlash, low weight, compactness, high torque capability, wide operating temperature range, and good repeatability. They also enable operations in low pressure environments (Putz, 2002). Despite the numerous advantages offered by these types of gear mechanisms, the main problem with harmonic drives is their significant joint flexibility. In addition to torsional flexibility in the gears, joint flexibility is caused by effects such as shaft windup and bearing deformation. In most cases, joint flexibility is the limiting factor to achieving satisfactory performance (Spong et al., 2006). As explained by Sasiadek (1992), the elastic vibrations of the joints, coupled with their large rotations and

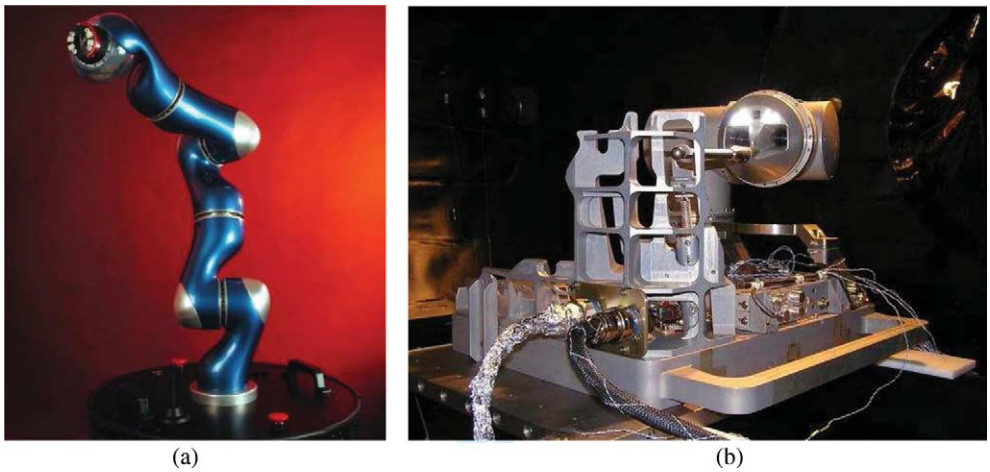

Figure 1. Lightweight robotic component demonstration experiments: (a) DLR Lightweight Robot III, and (b) ROKVISS experiment. Pictures courtesy of DLR (2010).

nonlinear dynamics, can also cause structural flexibility of the links. The coupling effects in a manipulator with both link and joint flexibilities have been investigated by several researchers (Yang and Donath, 1988; Lin and Gogate, 1989; Gogate and Lin, 1994; Xi et al., 1994; Xi and Fenton, 1994; Subudhi and Morris, 2002). As indicated by Sasiadek (2001), when the robotic arm is accelerated and stopped, large joint vibrations occur which makes the positioning of the tip very difficult. The astronauts' experience while handling the ISS robotic manipulators indicates that one has to wait several minutes for the manipulator's endpoint to stabilize. Hence, any operations would take much longer than in the case of a rigid manipulator. Impacts of flexibility effects on the control system performance of large scale robotic manipulators were highlighted by Cetinkunt and Book (1990). In some cases, joint flexibility can even lead to instability when neglected in the control design (Book, 1993). Because control schemes implemented onboard existing large robotic manipulators consist of very basic algorithms, the current solution to this problem consists of moving the manipulator's endpoint at a very low speed along a smooth trajectory to reduce the vibrations as much as possible (Sasiadek, 1997). For example, for the SSRMS robotic system the joint actuating control system consists of simple proportional-integral-derivative controllers that do not have the capability to efficiently damp residual vibrations at the joints.

For these reasons, several advanced control solutions have been proposed in the literature to address the flexible joint problem in the last few decades. For an exhaustive literature review on this topic, the reader is referred to the work of Ulrich and Sasiadek (2009). One of the approaches developed by the Canadian Space Agency to solve the flexible joint control problem includes a virtual decomposition-based adaptive strategy that uses joint torque measurements (Zhu and Doyon, 2004; Zhu et al., 2006). However, as noted by Ozgoli and Taghirad (2006), the design of a simple and efficient position controller, considering dynamics uncertainties in the presence of practical limitations such as the number of feasible measurements, is an area open for further investigation and development.

The objective of this paper is to demonstrate control of a two-link space robot manipulator modeled with rigid and flexible-joint dynamics and equipped only with motor and (or) link encoders and tachometers using two control schemes: a transpose jacobian (TJ) control strategy and a model reference adaptive control (MRAC) approach. The rigid-joint dynamics model is pursued further to account for flexible joints by first using a well-established linear spring model and second using a novel nonlinear-joint model. Both the rigid TJ and MRAC strategies were extended to these two flexible-joint dynamics models by applying the singular perturbation-based (SPB) theory to reduce transient joint vibrations in a large square trajectory-tracking scenario. Compared with other types of trajectories, such as straight lines or circles, large square trajectories represent an ideal case for studying the control of transient vibrations at the four orthogonal direction changes.

Manipulator dynamics

Robot configuration

The design and validation of the control systems are applied to the large two-link robot manipulator illustrated in **Figure 2,** which is equipped with a revolute shoulder joint having the capability to rotate over 2π rad and an elbow joint rotating $\pi/2$ rad in an elbow-down configuration. It is assumed that the robot has planar motion and that for space-based applications, gravity effects are neglected.

Rigid-joint robot dynamics

A conventional closed form of the nonlinear dynamics of a two-link robot manipulator with rigid joints is derived in terms of kinetic and potential energies, T_r and U_r, stored in the system by the Euler–Lagrange formulation (Asada and Slotine, 1986). Assuming that the kinetic energy of the robot is a quadratic function of the link angular rates and given the independent set of generalized set of coordinates $q_i = q_1$, $q_2, \ldots, q_n$, the nonlinear dynamics model of an n-link rigid robot is defined by the Lagrangian

$$L(q_i, \dot{q}_i) = T_r - U_r, \quad i = 1, \ldots, n \tag{1}$$

For a robot subjected to a generalized force τ_i acting on the generalized coordinates, the dynamics equations of motion are derived in the form given by

$$\tau_i = \frac{\mathrm{d}}{\mathrm{d}t}\left(\frac{\partial L}{\partial \dot{q}_i}\right) - \frac{\partial L}{\partial q_i}, \quad i = 1, \ldots, n \tag{2}$$

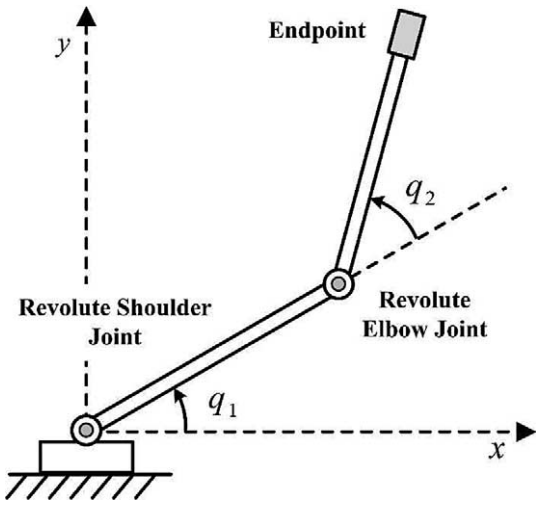

Figure 2. Two-link robotic manipulator.

For the two-link robot illustrated in **Figure 2**, the kinetic energy is given by

$$T_r = \frac{1}{2}\sum_{i=1}^{n}\sum_{j=1}^{n} M_{ij}\dot{q}_i\dot{q}_j = \frac{1}{2}\dot{\mathbf{q}}^T\mathbf{M}(\mathbf{q})\dot{\mathbf{q}},\ i=1,2; j=1,2; n=2 \tag{3}$$

where M_{ij} are the components of the $n \times n$ symmetric and positive definite rigid inertia matrix $\mathbf{M}(\mathbf{q})$ and $\mathbf{q}$ is the link angle vector. As mentioned earlier, gravitational energy is omitted for space applications. Substituting Equation (3) into Equation (2), and applying the differential operators, the following Euler–Lagrange rigid-dynamics equations of a n-DOF space robot is obtained

$$\boldsymbol{\tau} = \mathbf{M}(\mathbf{q})\ddot{\mathbf{q}} + \mathbf{C}(\mathbf{q},\dot{\mathbf{q}})\dot{\mathbf{q}} \tag{4}$$

where $\mathbf{C}(\mathbf{q},\dot{\mathbf{q}})$ comprises the Coriolis and centrifugal effects and $\boldsymbol{\tau}$ is the control torque vector. In the previous equation, $\mathbf{M}(\mathbf{q})$ and $\mathbf{C}(\mathbf{q},\dot{\mathbf{q}})$ are given by

$$\mathbf{M}(\mathbf{q}) = \begin{bmatrix} M_{11} & M_{12} \\ M_{21} & M_{22} \end{bmatrix} \tag{5}$$

$$\mathbf{C}(\mathbf{q},\dot{\mathbf{q}}) = -m_2 l_1 l_{c2}\sin q_2 \begin{bmatrix} \dot{q}_2 & \dot{q}_1+\dot{q}_2 \\ -\dot{q}_1 & 0 \end{bmatrix} \tag{6}$$

with

$$\begin{aligned} M_{11} &= m_1 l_{c1}^2 + m_2(l_1^2 + l_{c2}^2 + 2l_1 l_{c2}\cos q_2) + I_1 + I_2 \\ M_{12} &= M_{21} = m_2(l_{c2}^2 + l_1 l_{c2}\cos q_2) + I_2 \\ M_{22} &= m_2 l_{c2}^2 + I_2 \end{aligned} \tag{7}$$

where, $i = 1, 2$, q_i denotes the angular displacement of the revolute joints, l_i denotes the length of link i, l_{ci}, denotes the distance from the previous joint to the center of gravity of link i, and m_i denotes the mass of link i. The moment of inertia of link i about an axis perpendicular to the xy plane passing through the center of gravity of link i is denoted I_i.

Compared with other rigid-joint dynamics formulations, the nonlinear dynamics scheme presented in Equations (1) to (7) was chosen as it closely represents the nonlinear dynamical behaviour of a rigid-joint space manipulator and presents a great challenge for a trajectory tracking task. As noted by Green and Sasiadek (2004), other types of dynamics formulations, such linear state – state space models and fuzzy logic models do not capture efficiently multibody nonlinearities. Moreover, the selected nonlinear dynamics scheme can be further developed to include flexible effects.

Flexible-joint robot dynamics

In addition to the nonlinearity of rigid-joint dynamics, achieving accurate tracking control of the two-link robot with flexible joints is compounded by the elastic deformations at the joints and the associated vibrations. To enable the design of a suitable control strategy, the robot model must capture the nonlinear flexible dynamics of the robot and the control method must adequately dampen residual joint vibrations. The introduction of the constant joint stiffness matrix to model robot dynamics captures the interaction between joint vibrations and nonlinear multibody dynamics. By further considering time-varying stiffness coefficients, the soft-windup effect and friction torques revealed by experimental studies conducted on flexible-joint mechanisms provide a complete and accurate dynamics model that describes a flexible-joint manipulator system, which is presented in this section.

Linear-joint model

In the linear-joint dynamics model (Spong, 1987) each joint is modeled as a linear torsional spring of constant stiffness and the resulting dynamics of the flexible-joint manipulators consists of two second-order differential equations. Referring to **Figure 3**, let $\mathbf{q}_m$ be the vector denoting the angular displacements of the motor shaft angles, where the elastic joint vibrations vector is defined as $\mathbf{q}$–$\mathbf{q}_m$. The joint flexibility effect is taken into account by augmenting the kinetic energy of the rigid-joint space robot presented earlier with the kinetic energy of the rotors due to their own rotation and by considering the elastic potential energy of the flexible joints. The kinetic energy of the rotors, T_e, and the elastic potential energy, U_e, are given by

$$T_e = \frac{1}{2}\sum_{i=1}^{n}\sum_{j=1}^{n} J_{mij}\dot{q}_{mi}\dot{q}_{mj} = \frac{1}{2}\dot{\mathbf{q}}_m^T\mathbf{J}_m\dot{\mathbf{q}}_m,\ i=1,2; j=1,2; n=2 \tag{8}$$

$$\begin{aligned} U_e &= \frac{1}{2}\sum_{i=1}^{n}\sum_{j=1}^{n} k_{ij}(q_i - q_{mi})(q_j - q_{mj}) \\ &= \frac{1}{2}(\mathbf{q}-\mathbf{q}_m)^T\mathbf{k}(\mathbf{q}-\mathbf{q}_m), i = 1,2; j = 1,2; n = 2 \end{aligned} \tag{9}$$

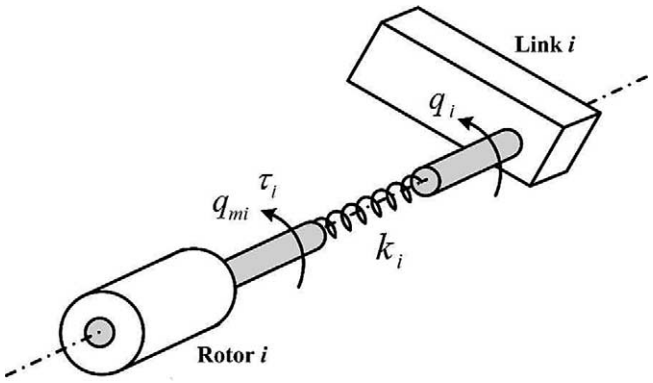

Figure 3. Flexible-joint modeling.

where $\mathbf{J}_m$ denotes the positive definite motor inertia matrix and where the stiffness of the flexible joints is modeled by the $\mathbf{k}$ matrix, the diagonal positive definite stifness matrix of the joints. Combining elastic terms with rigid-dynamics equations, the following dynamics equations of a flexible-joint space robot with revolute joints and actuated directly by DC motors are obtained:

$$\mathbf{M}(\mathbf{q})\ddot{\mathbf{q}} + \mathbf{C}(\mathbf{q},\dot{\mathbf{q}})\dot{\mathbf{q}} = \mathbf{k}(\mathbf{q}_m - \mathbf{q}) \tag{10}$$

$$\mathbf{J}_m\ddot{\mathbf{q}}_m + \mathbf{k}(\mathbf{q}_m - \mathbf{q}) = \boldsymbol{\tau} \tag{11}$$

In such a dynamics model, the link dynamics equation given by Equation (10) and the actuator dynamics equation given by Equation (12) are only coupled by the elastic torque term $\mathbf{k}(\mathbf{q}_m - \mathbf{q})$.

Nonlinear-joint model

Since the development of the linear stiffness model by Spong (1987) several researchers have conducted experiments to derive a detailed dynamics model of flexible effects in the joints of robotic manipulators. As nonlinear effects become prevalent in the system dynamics, their accurate modeling is key to the successful design of advanced flexible-joint control laws. The most relevant nonlinear effects are related to nonlinear stiffness. According to the literature, to replicate experimental joint stiffness curves, several studies recommend approximating the stiffness torque by a nonlinear cubic function. Another important characteristic related to nonlinear stiffness was demonstrated in experiments performed at the University of Toronto by Kircanski and Goldenberg (1997) who observed that the torque–torsion characteristic is deformed toward the torque axis in the region from 0 to 1 $N{\cdot}$m. In this region, the stiffness is lower due to the soft-windup effect.

Besides nonlinear-joint stiffness effects, friction torques have an important impact on the behavior of the robot manipulator system and need to be considered for accurate modeling and control. One of the most complete friction models was recently proposed by Makkar et al. (2005) that included all dominant friction components, i.e., static friction, Coulomb friction, viscous friction, and the Stribeck effect.

By combining the cubic nonlinear stiffness torque term, soft-windup effects, inertial coupling, and frictional torques, the following novel nonlinear-joint dynamics representation is obtained (Ulrich et al., 2012):

$$\mathbf{M}(\mathbf{q})\ddot{\mathbf{q}} + \mathbf{S}\ddot{\mathbf{q}}_m + \mathbf{C}(\mathbf{q},\dot{\mathbf{q}})\dot{\mathbf{q}} + \boldsymbol{f}(\dot{\mathbf{q}}) - \mathbf{k}(\mathbf{q},\mathbf{q}_m)(\mathbf{q}_m - \mathbf{q}) = \mathbf{0} \tag{12}$$

$$\mathbf{J}_m\ddot{\mathbf{q}}_m + \mathbf{S}^T\ddot{\mathbf{q}} + \mathbf{k}(\mathbf{q},\mathbf{q}_m)(\mathbf{q}_m - \mathbf{q}) = \boldsymbol{\tau} \tag{13}$$

where the nonlinear stiffness matrix $\mathbf{k}(\mathbf{q},\mathbf{q}_m)$is given by

$$\mathbf{k}(\mathbf{q},\mathbf{q}_m) = \mathbf{a}_1\begin{bmatrix}(q_{m1}-q_1)^2\\(q_{m2}-q_2)^2\end{bmatrix} + \mathbf{a}_2 + \mathbf{K}_{\mathrm{sw}}(\mathbf{q},\mathbf{q}_m) \tag{14}$$

where $\mathbf{a}_1$ and $\mathbf{a}_2$ are positive definite diagonal matrices of stiffness coefficients and $\mathbf{K}_{\mathrm{sw}}(\mathbf{q},\mathbf{q}_m)$ is the soft-windup correction factor that is modeled as a saddle-shaped function

$$\mathbf{K}_{\mathrm{sw}}(\mathbf{q},\mathbf{q}_m) = -\mathbf{k}_{\mathrm{sw}}\begin{bmatrix}e^{-a_{\mathrm{sw}}(q_{m1}-q_1)^2} & 0\\0 & e^{-a_{\mathrm{sw}}(q_{m2}-q_2)^2}\end{bmatrix} \tag{15}$$

with $\mathbf{k}_{\mathrm{sw}}$ and a_{sw} being parameters defining the soft-windup function. Consequently, the last term on the left side of Equation (12) is given by

$$\mathbf{k}(\mathbf{q},\mathbf{q}_m)(\mathbf{q}_m - \mathbf{q}) = \mathbf{a}_1\begin{bmatrix}(q_{m1}-q_1)^3\\(q_{m2}-q_2)^3\end{bmatrix} + \mathbf{a}_2(\mathbf{q}_m - \mathbf{q}) + \mathbf{K}_{\mathrm{sw}}(\mathbf{q},\mathbf{q}_m)(\mathbf{q}_m - \mathbf{q}) \tag{16}$$

In Equation (12), $\boldsymbol{f}(\dot{\mathbf{q}})$ denotes the friction torque assumed to have the following nonlinear parametrizable form

$$\boldsymbol{f}(\dot{\mathbf{q}}) = \gamma_1[\tanh(\gamma_2\dot{\mathbf{q}}) - \tanh(\gamma_3\dot{\mathbf{q}})] + \gamma_4\tanh(\gamma_5\dot{\mathbf{q}}) + \gamma_6\dot{\mathbf{q}} \tag{17}$$

where, for $i = 1, \ldots, 6$, yi denotes positive parameters defining the different friction components. In Equations (12) and (13), $\mathbf{S}$ denotes the strictly upper triangular matrix that models the inertial couplings between motor and link accelerations introduced by the dependency of the second rotor's kinetic energy on the first link's angular velocity.

Control schemes

Two rigid-joint control schemes were considered in this paper: one based on the TJ methodology and another one based on the MRAC technique. Then, these two rigid-joint control strategies were extended to include flexible-joint robot dynamics by applying the SPB theory. The distinction between the TJ and the MRAC control schemes was that with the adaptive one, the control gains were varied accordingly in real-time to the decentralized modified simple adaptive control (DMSAC) law to reduce the tracking error between the actual system outputs and the ideal system outputs specified in a reference model implemented on-board the robot system.

Rigid dynamics transpose jacobian control scheme

Because of its simplicity and ease of implementation onboard a space-qualified computer, the TJ control law was selected as the basis of further improvements and developments. Introduced by Craig (2005), the intuitive TJ control law provides a joint actuating torque vector given by

$$\boldsymbol{\tau} = \mathbf{J}(\mathbf{q})^T\left\{\mathbf{K}_p\begin{bmatrix}x_e\\y_e\end{bmatrix} + \mathbf{K}_d\begin{bmatrix}\dot{x}_e\\\dot{y}_e\end{bmatrix}\right\} \tag{18}$$

where $\mathbf{J}(\mathbf{q})$ is the robot Jacobian matrix and $\mathbf{K}_p$ and $\mathbf{K}_d$ are the proportional and derivative control gain matrix, respectively. Common to all control schemes is the use of link positions and velocities transformed in the direct

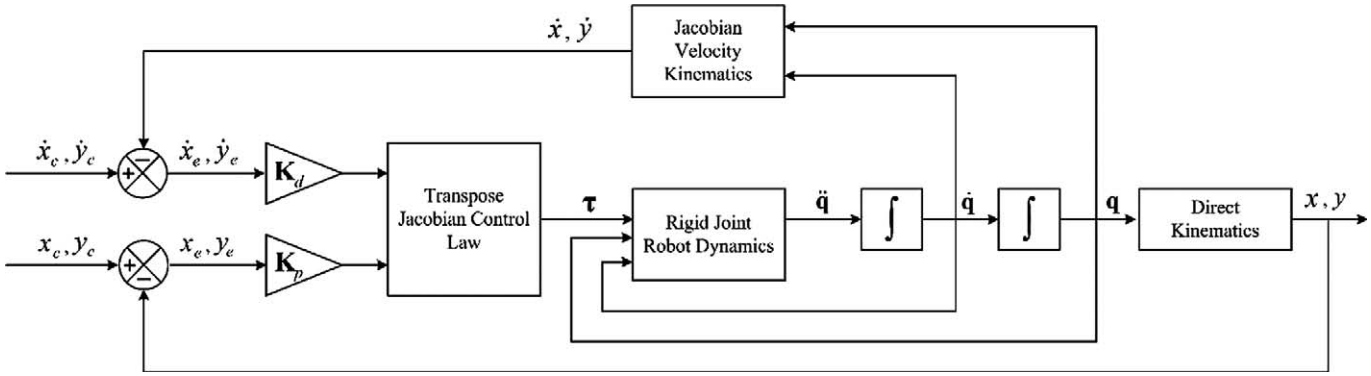

Figure 4. Rigid dynamics transpose jacobian control strategy.

kinematics and Jacobian velocity kinematics equations to provide the endpoint Cartesian position and velocity (Spong et al., 2006).

$$\begin{aligned} x &= l_1 \cos(q_1) + l_2 \cos(q_1 + q_2) \\ y &= l_1 \sin(q_1) + l_2 \sin(q_1 + q_2) \end{aligned} \tag{19}$$

$$\begin{aligned} \dot{x} &= -l_1 \dot{q}_1 \sin(q_1) - l_2(\dot{q}_1 + \dot{q}_2)\sin(q_1 + q_2) \\ \dot{y} &= l_1 \dot{q}_1 \cos(q_1) + l_2(\dot{q}_1 + \dot{q}_2)\cos(q_1 + q_2) \end{aligned} \tag{20}$$

As a function of the position tracking error x_e and y_e and velocity tracking error $\dot{x}_e$ and $\dot{y}_e$ defined as the difference between the commanded trajectory, $x_c, y_c, \dot{x}_c$, and $\dot{y}_c$, and the actual endpoint position and velocity, the control law given by Equation (18) computes the joint control torque vector to be applied to the space robot. The control torque actuating each joint feeds into the inverse rigid dynamics equations resulting in a joint angular acceleration vector $\ddot{\mathbf{q}}$, which is double integrated to obtain joint rates $\dot{\mathbf{q}}$ and joint angles $\mathbf{q}$. The block diagram of the rigid-joint control strategy is shown in **Figure 4**.

Rigid dynamics model reference adaptive control scheme

The rigid dynamics MRAC control scheme shown in **Figure 5** was investigated and presented in a previous work by Ulrich and Sasiadek (2010) and was inspired by the study of Sasiadek and Srinivasan (1988) for a single-link flexible manipulator. For the rigid-joint manipulator model, the proposed solution consists of time-varying the control gains $\mathbf{K}_p$ and $\mathbf{K}_d$ with the modified simple adaptive control law originally proposed by Ulrich and de Lafontaine (2007). To further reduce the number of computations, a local-decentralized approach was adopted, resulting in a DMSAC law given by the following adaptive control algorithm:

$$\boldsymbol{\tau} = \mathbf{J}(\mathbf{q})^T \left\{ \mathbf{K}_p(t) \begin{bmatrix} e_x \\ e_y \end{bmatrix} + \mathbf{K}_d(t) \begin{bmatrix} \dot{e}_x \\ \dot{e}_y \end{bmatrix} \right\} \tag{21}$$

where the adaptive control gains, $\mathbf{K}_p(t)$ and $\mathbf{K}_d(t)$, are adapted as the summation of a proportional and integral components (denoted with subscripts p and i, respectively), and accordingly with the DMSAC law, as follows

$$\mathbf{K}_p(t) = \mathbf{K}_{pp}(t) + \int \dot{\mathbf{K}}_{pi}(t)dt \tag{22}$$

$$\mathbf{K}_d(t) = \mathbf{K}_{dp}(t) + \int \dot{\mathbf{K}}_{di}(t)dt \tag{23}$$

with

$$\mathbf{K}_{pp}(t) = \begin{bmatrix} e_x^2 \Gamma_{pp} & 0 \\ 0 & e_y^2 \Gamma_{pp} \end{bmatrix} \tag{24}$$

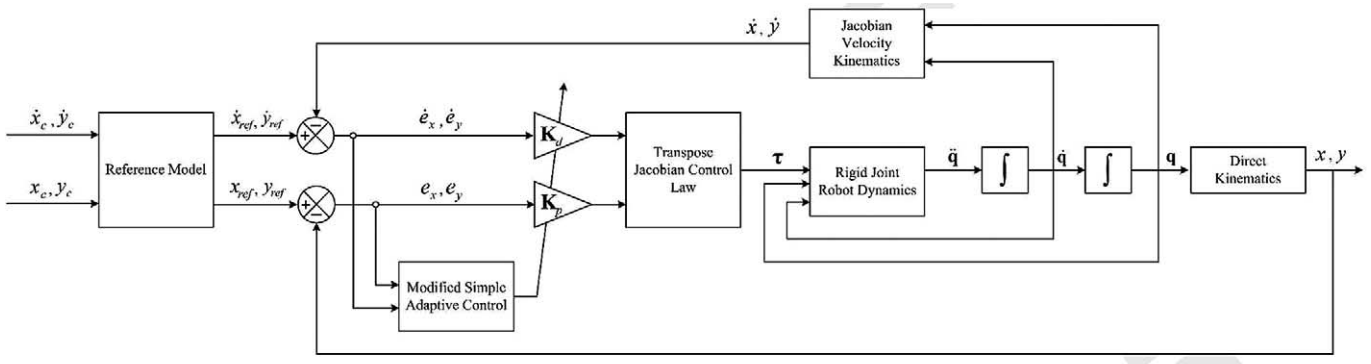

Figure 5. Rigid dynamics model reference adaptive control strategy.

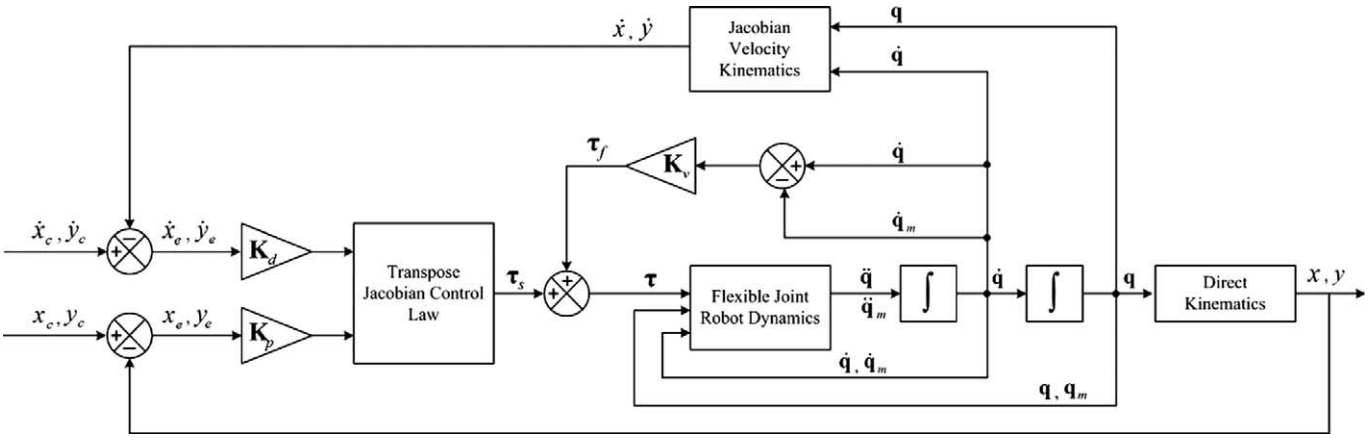

Figure 6. Flexible dynamics transpose jacobian control strategy.

$$\dot{\mathbf{K}}_{pi}(t) = \begin{bmatrix} e_x^2\Gamma_{pi} - \sigma_p K_{pi11}(t) & 0 \\ 0 & e_y^2\Gamma_{pi} - \sigma_p K_{pi22}(t) \end{bmatrix} \quad (25)$$

$$\mathbf{K}_{dp}(t) = \begin{bmatrix} \dot{e}_x^2\Gamma_{dp} & 0 \\ 0 & \dot{e}_y^2\Gamma_{dp} \end{bmatrix} \quad (26)$$

$$\dot{\mathbf{K}}_{di}(t) = \begin{bmatrix} \dot{e}_x^2\Gamma_{di} - \sigma_d K_{di11}(t) & 0 \\ 0 & \dot{e}_y^2\Gamma_{di} - \sigma_d K_{di22}(t) \end{bmatrix} \quad (27)$$

In Equations (24) to (27), Γ_{pp}, Γ_{pi}, Γ_{dp}, and Γ_{di} are control parameters that control the rate of adaptation and σ_p and σ_d are small and positive forgetting control coefficients necessary to avoid divergence of the integral control gains. Without the σ terms, the integral adaptive gains could increase indefinitely as long as a tracking error exists. The reference model, which was modeled by a set of second-order uncoupled linear transfer functions of the form

$$G(s) = \frac{\omega_n^2}{s^2 + 2\zeta\omega_n s + \omega_n^2} \quad (28)$$

represents the ideal closed-loop system. As shown in **Figure 5**, the output vector of this ideal system, x_{ref}, y_{ref}, $\dot{x}_{\text{ref}}$, and $\dot{y}_{\text{ref}}$ was compared with the actual endpoint position and velocity, x, y, $\dot{x}$, and $\dot{y}$, respectively, to form the tracking errors between them, e_x, e_y, $\dot{e}_x$, and $\dot{e}_y$. These tracking errors were used in the adaptive control law given by Equation (21) and in the adaptation law used to vary the control gains in real time, as shown in Equations (24) to (27).

Flexible dynamics transpose jacobian control scheme

Recently, Ulrich et al. (2012) showed that the control law given by Equation (18), which achieves stable tracking of a commanded trajectory under the assumption of perfect rigidity, can be extended to control flexible-joint robot systems. Specifically, the strategy consisted of using the SPB theory. Applied to flexible-joint robots, this theory provides a way to design composite controllers, in which a fast control term that damps the elastic vibrations at the joints is added to a slow control term which controls the rigid dynamics. Generally, a composite control law is of the form

$$\boldsymbol{\tau} = \boldsymbol{\tau}_s + \boldsymbol{\tau}_f \quad (29)$$

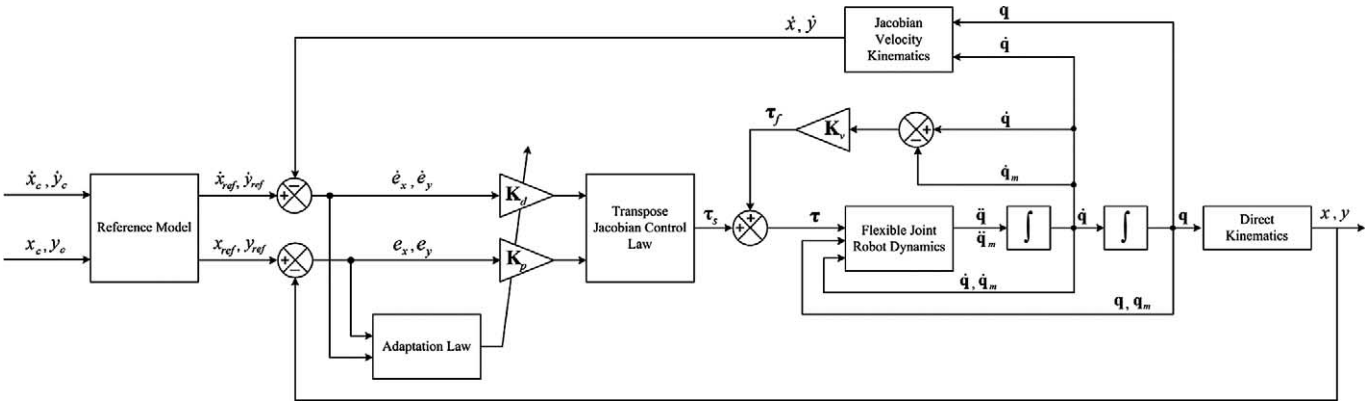

Figure 7. Flexible dynamics model reference adaptive control strategy.

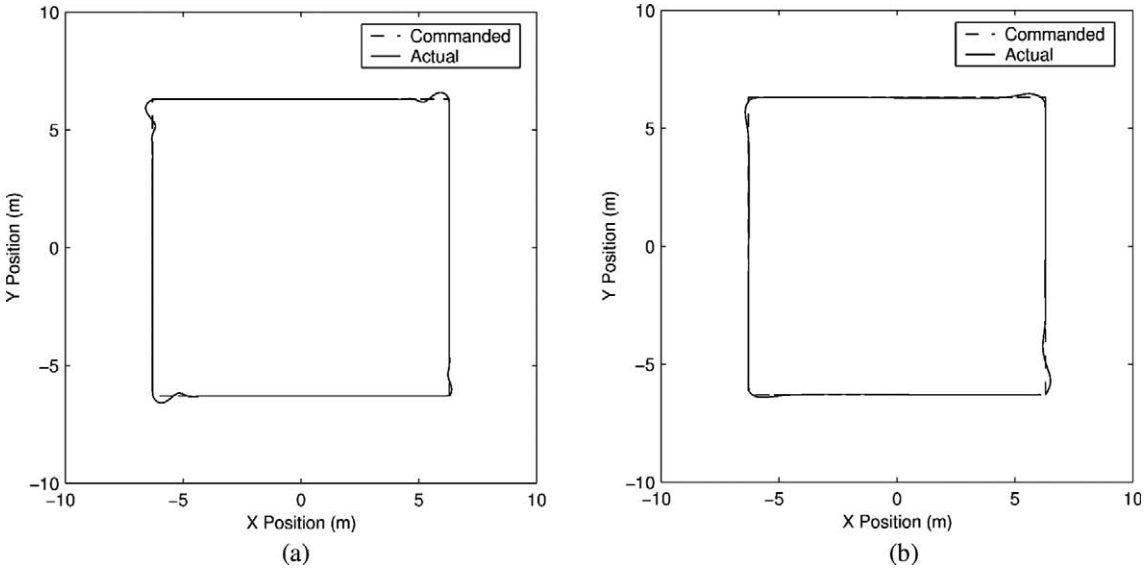

Figure 8. Rigid dynamics trajectories: (a) rigid transpose jacobian control scheme, and (b) rigid model reference adaptive control scheme (Ulrich and Sasiadek, 2010).

where τ_s is designed to control the slow (or rigid) dynamics and τ_f is designed to stabilize the fast (or flexible) dynamics. In this paper, the fast control term was chosen as a linear correction of the form $\mathbf{K}_v(\dot{\mathbf{q}} - \dot{\mathbf{q}}_m)$ and the rigid control term consists of the rigid nonadaptive control law given by Equation (18). The resulting flexible nonadaptive control law is defined as

$$\boldsymbol{\tau} = \mathbf{J}(\mathbf{q})^T \left\{ \mathbf{K}_p \begin{bmatrix} x_e \\ y_e \end{bmatrix} + \mathbf{K}_d \begin{bmatrix} \dot{x}_e \\ \dot{y}_e \end{bmatrix} \right\} + \mathbf{K}_v(\dot{\mathbf{q}} - \dot{\mathbf{q}}_m) \tag{30}$$

Similar to the rigid control strategies, the first term of the control law given by Equation (30) computes the slow control torque vector as a function of the position tracking errors, x_e and y_e, and velocity tracking errors, $\dot{x}_e$ and $\dot{y}_e$. This control term is added to the fast control term which is obtained as a function of $\mathbf{K}_v$ and the link and motor angular velocity differences. The total control torque actuating each joint feedsinto the inverse flexible-joint dynamics equations resulting in a link and motor angular acceleration vectors, $\ddot{\mathbf{q}}$ and $\ddot{\mathbf{q}}_m$, which are double integrated to obtain link and motor rates, $\dot{\mathbf{q}}$ and $\dot{\mathbf{q}}_m$, and link and motor angular positions, $\mathbf{q}$ and $\mathbf{q}_m$. The complete block diagram of the flexible TJ control strategy is illustrated in **Figure 6**.

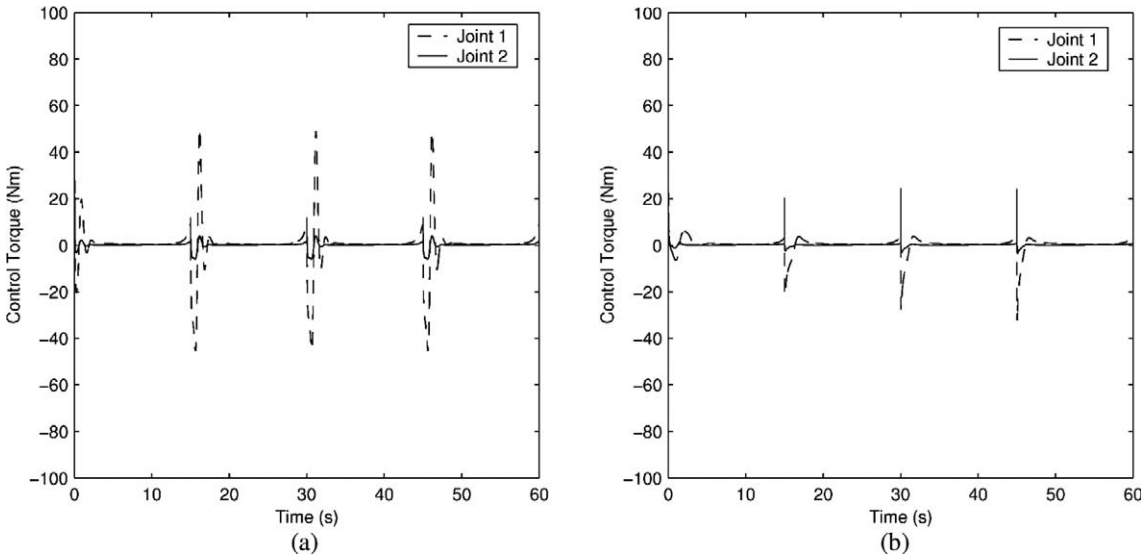

Figure 9. Rigid dynamics control torques: (a) rigid transpose jacobian control scheme, and (b) rigid model reference adaptive control scheme.

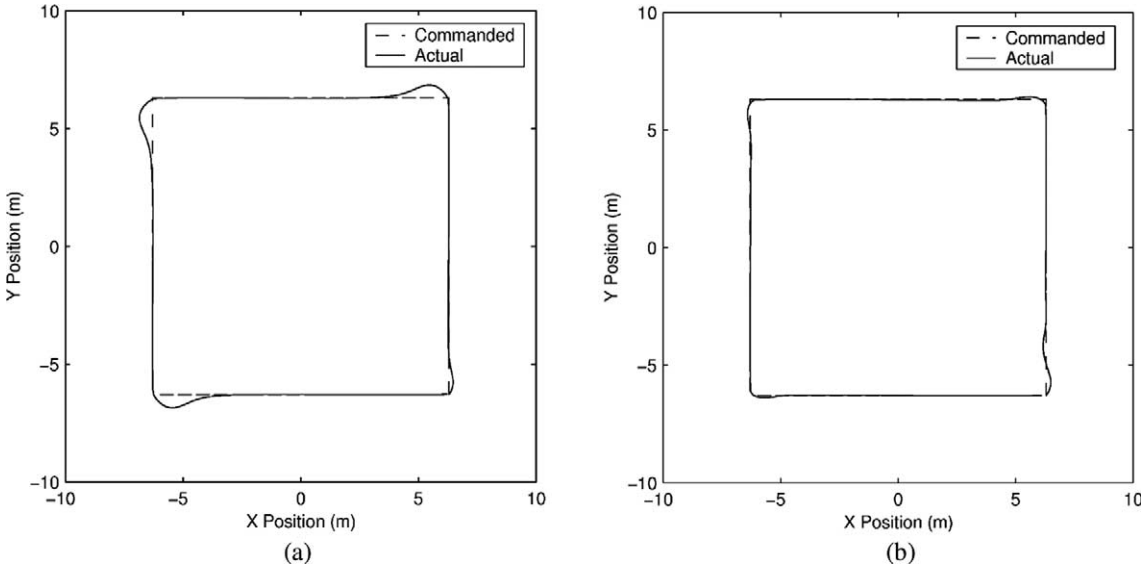

Figure 10. Linear-joint dynamics trajectories: (a) flexible transpose jacobian control scheme, and (b) flexible model reference adaptive control scheme (Ulrich et al., 2012).

Flexible dynamics model reference adaptive control scheme

The adaptive extension of the flexible control law described by Equation (30) was proposed by Ulrich et al. (2012) and is illustrated in **Figure 7**. Similar to the rigid dynamics MRAC strategy described earlier, adaptive control was achieved by time-varying the control gains $\mathbf{K}_p$ and $\mathbf{K}_d$ with the DMSAC adaptation law. The resulting flexible adaptive control scheme is given by

$$\boldsymbol{\tau} = \mathbf{J}(\mathbf{q})^T \left\{ \mathbf{K}_p(t) \begin{bmatrix} e_x \\ e_y \end{bmatrix} + \mathbf{K}_d(t) \begin{bmatrix} \dot{e}_x \\ \dot{e}_y \end{bmatrix} \right\} + \mathbf{K}_v(\dot{\mathbf{q}} - \dot{\mathbf{q}}_m) \qquad (31)$$

Simulation results

This section summarizes the results obtained by implementing the rigid control laws to the rigid-joint dynamics and by implementing the flexible control laws to both the linear and the nonlinear flexible-joint dynamics models. The physical properties of the robot (the length and the mass of the links) were adopted form previous studies on intelligent control of space robots (Green and Sasiadek, 2005), and the parameters for the linear-joint model were adopted from Cao and de Silva (2006), which are representative of highly flexible joints. The parameters of

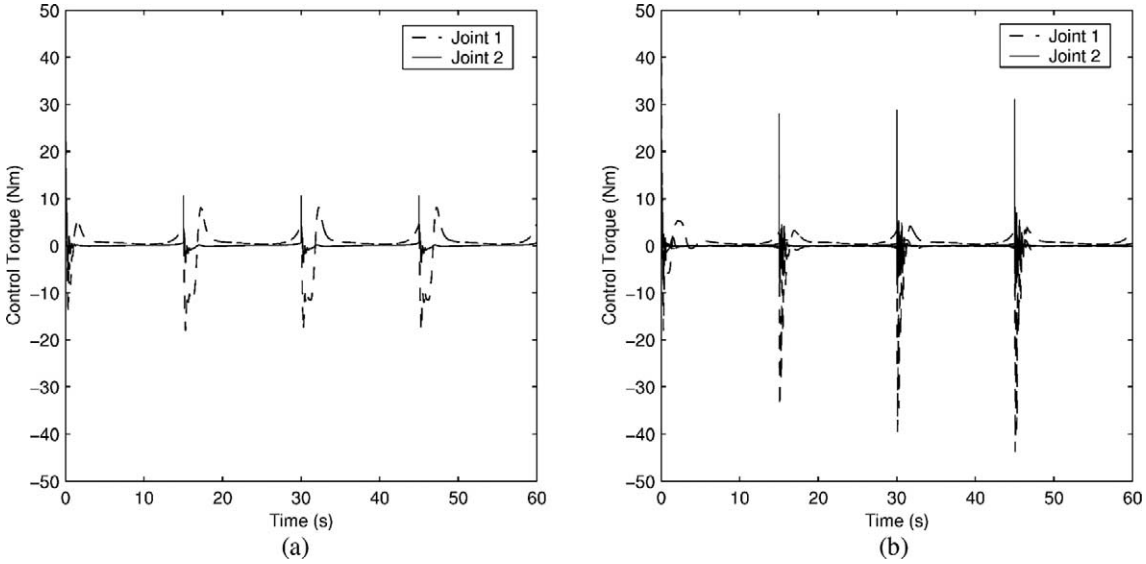

Figure 11. Linear-joint dynamics control torques: (a) flexible transpose jacobian control scheme, and (b) flexible model reference adaptive control scheme.

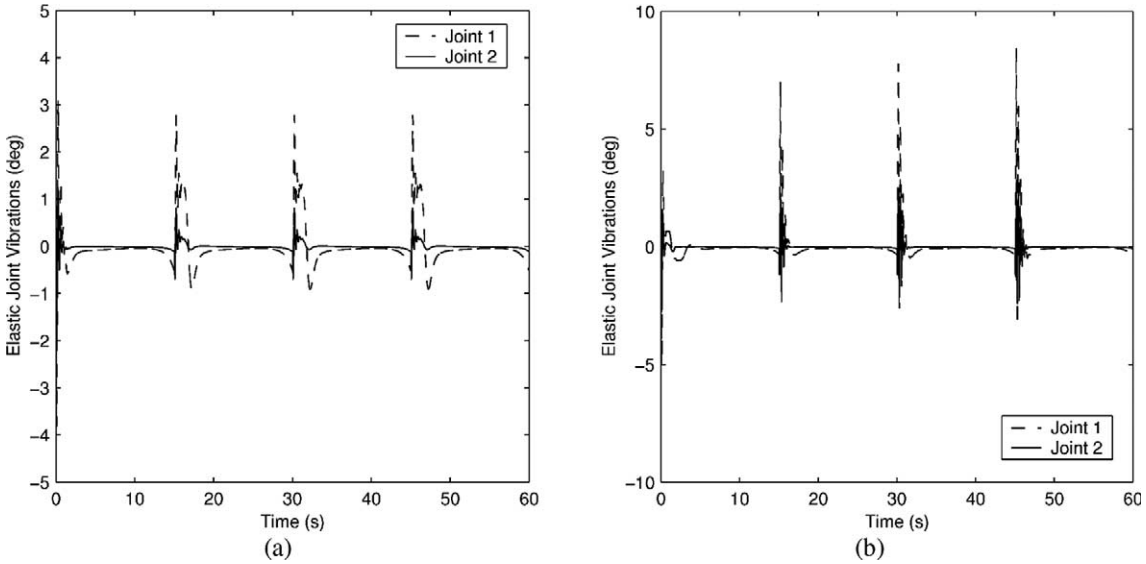

Figure 12. Linear-joint dynamics vibrations: (a) flexible transpose jacobian control scheme, and (b) flexible model reference adaptive control scheme.

the two-link flexible-joint robot are summarized as follows: $l_1 = l_2 = 4.5$ m, $m_1 = m_2 = 1.5075$ kg, $J_{m1} = J_{m2} = 1$ kg·m^2 and $k_1 = k_2 = 500$ N·m/rad. For the nonlinear-joint model, the parameters were taken from Ulrich et al. (2012). The constant proportional and derivative gains for the rigid dynamics TJ controller were calculated from the manipulator dynamics (Green, 2007), whereas the gains for the flexible dynamics TJ controller were selected as $\mathbf{K}_p = \text{diag}[7]$, $\mathbf{K}_d = \text{diag}[10]$, and $\mathbf{K}_v = \text{diag}[35]$. The rigid adaptive control parameters were selected as $\Gamma_{pp} = 120$, $\Gamma_{pi} = 180$, $\Gamma_{pi} = 180$, $\Gamma_{dp} = 15$, $\Gamma_{di} = 30$ and $\sigma_p = \sigma_i = 0.018$ and the flexible adaptive control parameters as $\Gamma_{\text{pp}} = \Gamma_{pi} = 150$, $\Gamma_{\text{pp}} = \Gamma_{pi} = 150$, $\Gamma_{dp} = \Gamma_{di} = 25$, $\sigma_p = 0.008$, and $\sigma_d = 0.023$. In both cases, the adaptation algorithm was activated with $\mathbf{K}_{pi}(0) = \mathbf{K}_{di}(0) = \mathbf{0}_{2\times 2}$. The reference model parameters were chosen as $\omega_n = 10$ rad/s and $\zeta = 0.9$. The rigid dynamics MRAC control gains were selected in numerical simulation to provide optimal tracking results for the rigid joint manipulator. Similarly, the flexible TJ and MRAC control gains, parameters, and coefficients were selected in numerical simulations to provide optimal tracking results

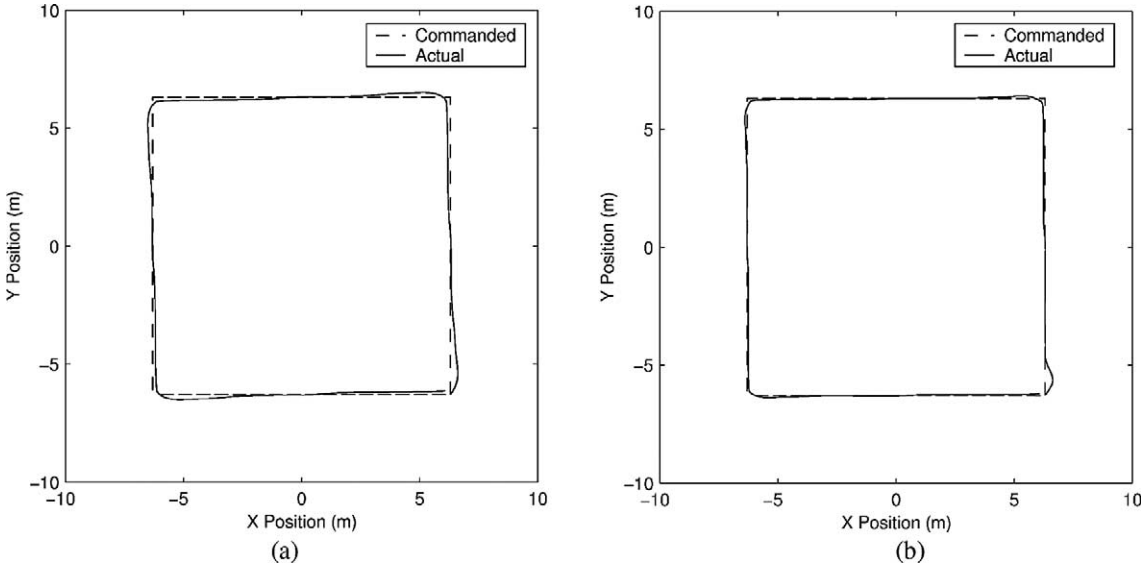

Figure 13. Nonlinear-joint dynamics trajectories: (a) flexible transpose jacobian control scheme, and (b) flexible model reference adaptive control scheme (Ulrich et al., 2012).

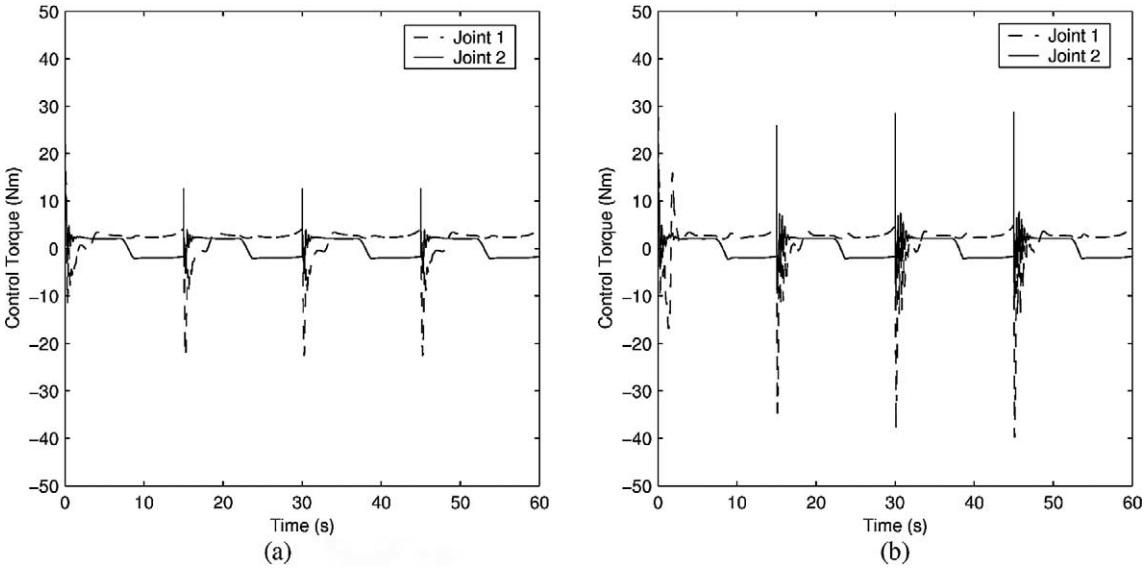

Figure 14. Nonlinear-joint dynamics control torques: (a) flexible TJ control scheme, and (b) flexible model reference adaptive control scheme.

for the two-link flexible-joint space robot modeled with the linear-joint dynamics model described earlier, i.e., with constant joint stiffness coefficients.

Figures 8, **10**, and **13** show the results obtained for tracking a 12.6 m $\times$ 12.6 m square trajectory in 60 s in a counterclockwise direction starting from rest at the lower right corner, where the solid lines represent the endpoint actual position and the dashed lines the commanded position. The manipulator does not fully extend during the tracking operation and remains in the elbow-down configuration. Compared with other types of trajectories, such as straight lines or circles, large square trajectories represent an ideal case for studying the control of transient vibrations at the four orthogonal direction changes.

The rigid dynamics trajectory obtained with the rigid TJ control trajectory shown in **Figure 8a** exhibits pronounced overshoots of 0.29 m at each direction change, compared with the rigid MRAC approach shown in **Figure 8b,** which exhibits minimal overshoots of 0.15 m, 0.13 m, and 0.10 m for the first, second and third direction change, respectively. Moreover, these much improved trajectory tracking results over the TJ controller are obtained at smaller control efforts, as shown in **Figure 9**, which illustrates the control torques for both control strategies.

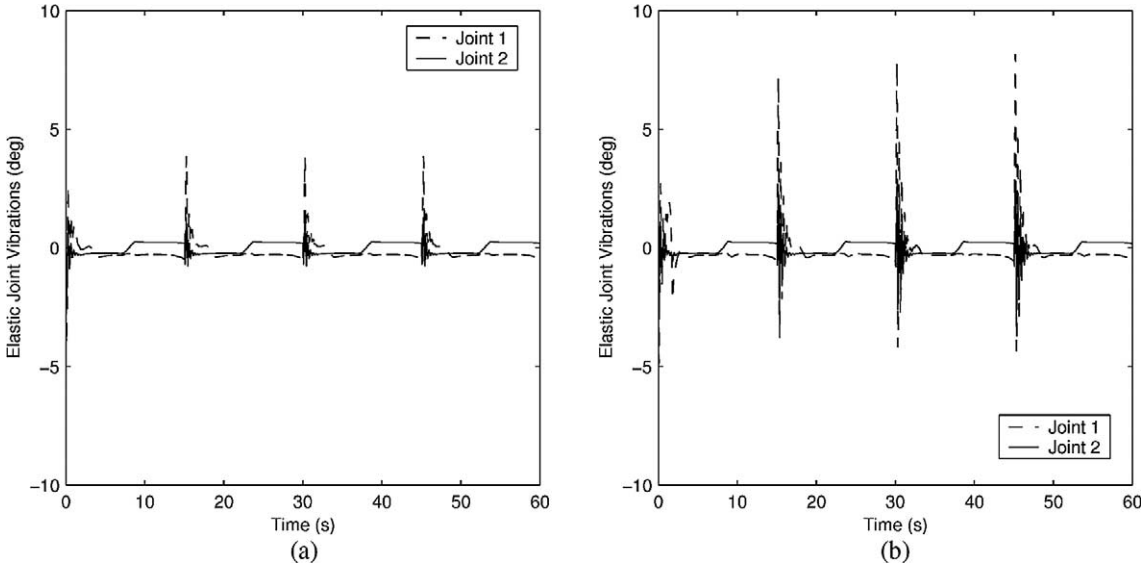

Figure 15. Nonlinear-joint dynamics vibrations: (a) flexible transpose jacobian control scheme, and (b) flexible model reference adaptive control scheme.

As illustrated in **Figure 10a**, the linear-joint dynamics trajectory obtained with the flexible TJ control undergoes larger overshoots than that of the rigid TJ control case, on the order of 0.35 m at each direction change. These poor tracking results are explained by the weak damping of the elastic joint vibration effects which are included in the linear-joint dynamics model, as shown in **Figure 12a** where the elastic joint vibration vector is defined as $\mathbf{q}–\mathbf{q}_m$. On the other hand, as illustrated in **Figure 10b**, the adaptive strategy provides improved tracking results, with overshoots of 0.11 m, 0.10 m and 0.08 m for the first, second and third direction change, respectively. Moreover, the flexible adaptive controller exhibits rapid settling to a steady-state, such that tracking is close to a straight line along each side of the trajectory. As shown in **Figure 12b**, the elastic vibrations obtained with the flexible MRAC strategy are also quickly damped. Hence, the response obtained with the adaptive solution is much closer to a perfect square than the TJ response. However, these improvements in tracking performance are obtained at the expense of higher control torques, as demonstrated in **Figure 11**.

The results obtained in terms of trajectory tracking, control torques, and resulting elastic joint vibrations, by applying both flexible control techniques to the nonlinear-joint dynamics model are shown in **Figures 13**, **14**, and **15**, respectively. Similar to the case where both controllers were applied to the linear-joint dynamics model, the flexible MRAC strategy yielded minimal overshoots at each direction change compared with the flexible TJ strategy. This is shown in **Figure 13** where an overshoot of 0.20 m occurs at each corner of the trajectory for the TJ scheme compared with 0.11 m, 0.09 m, and 0.08 m at the first, second, and third direction change, respectively, for the MRAC approach. However, the gain in tracking performance came again at the expense of higher control efforts. Both flexible controllers were tuned in numerical simulations using the linear-joint dynamics formulation. Hence, the tracking results shown in **Figure 13** can be interpreted as an indication of the robustness of the proposed controllers to uncertainties in the manipulator dynamics model. Results obtained with other nonlinear trajectory tracking control schemes tested for the same square trajectory, flexible-joint robot manipulator, and control objectives (Ulrich and Sasiadek, 2011) did not compare favorably with the results shown in this paper. All simulations were conducted using MATRIXx, National Instruments' software suite for model-based control system design.

Conclusion

In this paper, the relative effectiveness in tracking a square trajectory by a two-link space manipulator described by a rigid-joint nonlinear dynamics model was demonstrated with two techniques: a TJ method and a MRAC approach in which the gains were adapted in real-time using the DMSAC approach. Although these two controllers provide stable closed-loop behavior when applied to the two-link rigid-joint robot model, the MRAC scheme exhibited rapid settling to a steady state with minimum overshoots at each corner of the square trajectory, hence yielding better tracking performance. The rigid dynamics model was used initially to establish a benchmark in system response and to assess the applicability of advanced control schemes to study flexible-joint space manipulator dynamics models.

The rigid-joint dynamics model was further developed to include flexible effects in the joints by using the well-established Euler–Lagrange formulation, which resulted in a dynamics model characterized by two second-order differential equations in which the joints were described by a linear torsional spring of constant stiffness. Using this dynamics formulation, an extension of the two control approaches were developed using the SPB theory. Similar to the rigid control schemes, the flexible TJ strategy provided poor tracking performance compared with the flexible MRAC solution.

Finally, a detailed and more realistic dynamics model for flexible-joint space manipulators in which nonlinear stiffness, soft-windup, and frictional effects are considered was reviewed. Although such a highly nonlinear model presented additional control challenges, the MRAC strategy achieved higher precision control with minimal overshoots at each corner of the trajectory.

Future work could pursue the development of other advanced trajectory tracking control strategies suitable for rigid and flexible-joint space robots such as nonlinear optimal and fuzzy control techniques and compare their performance with the ones presented in this study.

Acknowledgements

This work was partially funded by the Natural Sciences and Engineering Research Council of Canada (NSERC) under the Alexander Graham Bell Canada Graduate Scholarship (CGS) CGS D3-374291-2009. Financial assistance from the Canadian Space Agency, the Canadian Armed Forces, the Faculty of Engineering and Design and the Faculty of Graduate Studies and Research at Carleton University is also gratefully acknowledged.

References

Asada, H., and Slotine, J.J.E. 1986. *Robot analysis and control*. John Wiley and Sons.

Book, W.J. 1993. Structural flexibility of motion systems in the space environment. *IEEE Transactions on Robotics and Automation*, Vol. 9, No. 5, pp. 524–530, 1993. doi: 10.1109/70.258045.

Cao, Y., and de Silva, C.W. 2006. Dynamic modeling and neural-network adaptive control of a deployable manipulator system. *Journal of Guidance, Control, and Dynamics*, Vol. 29, No. 1, pp. 192–194. doi: 10.2514/1.11032.

Cetinkunt, S., and Book, W.J. 1990. Flexibility effects on the control system performance of large scale robotic manipulators. *Journal of the Astronautical Sciences*, Vol. 38, No. 4, pp. 531–556.

Craig, J.J. 2005. *Introduction to robotics: mechanics and control*. Prentice Hall, Upper Saddle River, NJ, 3rd edition.

DLR. 2010. Institute of robotics and mechatronics – lightweight robots. Available at: http://www.dlr.de/rm/en/desktopdefault.aspx/tabid-3803/ [accessed 25 March 2012].

Ellery, A. 2000. *An introduction to space robotics*. Springer-Verlag New York Inc.

Gogate, S., and Lin, Y.J. 1994. Modeling and control of a deformable-link flexible joint robot. *International Journal of Systems Science*, Vol. 25, No. 2, pp. 237–251. doi: 10.1080/00207729408928957.

Green, A. 2007. Intelligent tracking control of fixed-base and free flying flexible space robots. PhD thesis, Department of Mechanical and Aerospace Engineering, Carleton University, Ottawa, Ontario.

Green, A., and Sasiadek, J.Z. 2004. Dynamics and trajectory tracking control of a two-link robot manipulator. *Journal of Vibration and Control*,. Vol. 10, No. 10. pp. 1415–1440. doi: 10.1177/10775463 04042058.

Green, A., and Sasiadek, J.Z. 2005. Adaptive control of a flexible robot using fuzzy logic. *Journal of Guidance, Control, and Dynamics*, Vol. 28, No. 1, pp. 36–42. doi: 10.2514/1.6376.

Kircanski, N.M., and Goldenberg, A.A. 1997. An experimental study of nonlinear stiffness, hysteresis, and friction effects in robot joints with harmonic drives and torque sensors. *The International Journal of Robotics Research*, Vol. 16, No. 2, pp. 214–239. doi: 10.1177/027 836499701600207.

Lin, Y.J., and Gogate, S.D. 1989. Modeling and motion simulation of an *n*-link flexible robot with elastic joints. In *Proceedings of the International Symposium on Robotics and Manufacture*, Santa Barbara, CA, 4–8 October.

Makkar, C., Dixon, W.E., Sawyer, W.G., and Hu, G. 2005. A new continuously differentiable friction model for control systems design. In *Proceedings of the 2005 IEEE/ASME International Conference on Advanced Intelligent Mechatronics*, Monterey, CA, 24–28 July.

Ozgoli, S., and Taghirad, H.D. 2006. A survey on the control of flexible joint robots. *Asian Journal of Control*, Vol. 8, No. 4, pp. 332–344. doi: 10.1111/j.1934-6093.2006.tb00285.x.

Putz, P. 2002. Space robotics. *Reports on Progress in Physics*, Vol. 65, No. 3, pp. 421–463. doi: 10.1088/0034-4885/65/3/202.

Reintsema, D., Landzettel, K., and Hirzinger, G. 2007. DLRs advanced telerobotic concepts and experiments for on-orbit servicing. In *Advances in Telerobotics*, edited by M. Ferre, M. Buss, R. Aracil, C. Melchiorri, and C. Balaguer. Vol. 31 of Springer Tracts on Advanced Robotics, Springer-Verlag Berlin Heidelberg.

Salaberger, C. 1998. Canadian space robotic activities. *Acta Astronautica*, Vol. 41, No. 4, pp. 239–246. doi: 10.1016/S0094-5765(98)00082-4.

Sasiadek, J.Z., and Srinivasan, R. 1988. Dynamics modeling and adaptive control of a single-link flexible manipulator. *Journal of Guidance, Control and Dynamics*, Vol. 12, No. 6, pp. 838–844. doi: 10.2514/3.20489.

Sasiadek, J.Z. 1992. Space robotics and manipulators: lessons learned from the past and future missions and systems. In *Proceedings of the 12th International IFAC Symposium on Automatic Control in Aerospace*, Ottobrunn, Germany, 7–11 September.

Sasiadek, J.Z. 1997. Space robotics and manipulators – the past and the future. *Control Engineering Practice*, Vol. 2, No. 3, pp. 491–497. doi: 10.1016/0967-0661(94)90787-0.

Sasiadek, J.Z. 2001. Preface to the special section on space robotics. *Control Engineering Practice*, Vol. 9, No. 2, pp. 189–190. doi: 10.1016/ S0967-0661(00)00105-2.

Spong, M.W. 1987. Modeling and control of elastic joint robots. *Journal of Dynamic Systems, Measurement and Control*, Vol. 109, No. 4, pp. 310–319. doi: 10.1115/1.3143860.

Spong, M.W., Hutchinson, S., and Vidyasagar, M. 2006. *Robot modeling and control*. John Wiley and Sons, New York, NY.

Subudhi, B., and Morris, A.S. 2002. Dynamic modeling, simulation and control of a manipulator with flexible links and joints. *Robotics and Autonomous Systems*, Vol. 41, No. 4, pp. 257–270. doi: 10.1016/S0921-8890(02)00295-6.

Ulrich, S., and de Lafontaine, J. 2007. Autonomous atmospheric entry on Mars: performance improvement using a novel adaptive control algorithm. *Journal of the Astronautical Sciences*, Vol. 55, No. 4, pp. 431–449.

Ulrich, S., and Sasiadek, J.Z. 2009. Autonomous control for flexible joint space robotic manipulators. In *Proceedings of the 60th International Astronautical Congress*, Daejeon, Republic of Korea, 12–16 October.

Ulrich, S., Sasiadek, J.Z., and Barkana, I. 2012. Modeling and direct adaptive control of a flexible-joint manipulator, *Journal of Guidance, Control and Dynamics*, Vol. 35, No. 1, pp. 25–39. doi: 10.2415/1.54083.

Ulrich, S., and Sasiadek, J.Z. 2010. Modified simple adaptive control for a two-link space robot. In *Proceedings of the American Control Conference*, Baltimore, MD, 30 June–2 July.

Ulrich, S., and Sasiadek, J.Z. 2011. Methods of trajectory tracking for flexible-joint space manipulators," In *Proceedings of 18th IFAC World Congress*, Milan, Italy, 28 August–2 September.

Xi, F., and Fenton, R.G. 1994. Coupling effect of a flexible link and a flexible joint. *International Journal of Robotics Research*, Vol. 13, No. 4, pp. 443–453. doi: 10.1177/027836499401300505.

Xi, F., Fenton, R.G., and Tabarrok, B. 1994. Coupling effects in a manipulator with both a flexible link and joint. *Journal of Dynamic Systems, Measurement and Control*, Vol. 116, No. 4, pp. 826–831. doi: 10.1115/1.2899288.

Yang, G.B., and Donath, M. 1988. Dynamic model of a one-link robot manipulator with both structural and joint flexibility. In *Proceedings of the IEEE International Conference on Robotics and Automation*, Philadelphia, PA, 24–29 April.

Zhu, W.-H., and Doyon, M. 2004. Adaptive control of harmonic drives. In *43rd IEEE Conference on Decision and Control*, Atlantis Paradise Island, Bahamas.

Zhu, W.-H., Dupuis, E., Doyon, M., and Piedboeuf, J.-C. 2006. Adaptive control of harmonic drives based on virtual decomposition. *IEEE/ ASME Transactions on Mechatronics*, Vol. 11, No. 5, pp. 604–614. doi: 10.1109/TMECH.2006.882992.